PCCP

PAPER

View Article Online
View Journal | View Issue

Cite this: *Phys. Chem. Chem. Phys.*, 2022, **24**, 13534

First-order hyperpolarizabilities of propellanes: elucidating structure–property relationships†

Bartosz Krajewski,[a] Swati Singh Rajput,[b] Marta Chołuj,[c] Elżbieta Wojaczyńska,[c] Andrzej Miniewicz,[c] Md. Mehboob Alam *[b] and Robert Zaleśny *[c]

Received 24th January 2022,
Accepted 5th May 2022

DOI: 10.1039/d2cp00381c

rsc.li/pccp

Following recent experimental work demonstrating strong nonlinear optical properties, namely second harmonic generation of light, in crystals composed of 16,20-dinitro-(3,4,8,9)-dibenzo-2,7-dioxa-5,10-diaza[4.4.4]propellane molecules [A. Miniewicz, S. Bartkiewicz, E. Wojaczyńska, T. Galica, R. Zaleśny and R. Jakubas, *J. Mater. Chem. C*, 2019, **7**, 1255–1262] in this paper we aim to investigate "structure–property" relationships for a series of 16 propellanes presenting a wide palette of substituents with varying electron-accepting/donating capabilities. To that end, we use electronic- and vibrational-structure theories and a recently developed generalized few-state model combined with a range-separated CAM-B3LYP functional to analyze electronic and vibrational contributions to the first hyperpolarizability for the whole series of molecules. The variations in computed properties are large among the studied set of substituents and can reach an order of magnitude. It has been demonstrated that the maximum values of frequency-independent first hyperpolarizability are expected for strong electron-accepting NO_2 substituents, but only at the preferred position with respect to the electronegative oxygen atom in the 1,4-oxazine moiety. This holds for electronic as well as vibrational counterparts.

1 Introduction

Propellanes are molecular systems owing their name to the propeller-like structure. In the case of smaller members of the family, the three rings connected through a common covalent bond cause very strained and unstable geometries. Owing to this, propellanes undergo polymerization to produce interesting structures such as staffanes. Snatzke and Zanati were the first to synthesize propellane in 1965.[1] Propellanes, however, have been presumably obtained in some earlier preparations.[2,3] The name "propellane" was first used by Ginsberg in 1966.[4] Since then, several research groups have synthesized and studied the properties of different propellanes including heteropropellanes – where the ring structures are not necessarily hydrocarbons.[5–11]

Apart from their strained geometry, propellanes are popular due to their diverse applications in synthetic chemistry ranging from materials to natural products.[5] It is important to note that although the research on propellanes started about 80 years ago, these systems are very common in natural products. Propellanes containing larger rings are stable enough to provide a platform for designing desired molecular structures such as for highly efficient organic light-emitting diodes.[12] The common covalent bond in propellanes can easily be broken and the resultant valency can be satisfied by different groups. In this way, the unstrained propellane moiety can be attached to different types of molecular entities (*e.g.* during polymerization). This provides a number of possibilities in synthetic chemistry.[13,14] The preparation of staffanes and various dendrimers essentially involves the breaking of the said common covalent bond.[5,15] These experimental advances were supported, in parallel, by the theoretical studies[5,16–19] on propellanes. However, these studies were limited to strain energy, the mechanism of the polymerization reaction of propellane, and singlet–triplet transition, to name a few.

In spite of numerous applications of various propellanes in organic synthesis, there are very few studies focusing on nonlinear optical properties of such compounds. Very recently, some of the present authors have synthesized a heteropropellane-based molecule, 16,20-dinitro-(3,4,8,9)-dibenzo-2,7-dioxa-5,10-diaza[4.4.4]propellane (DDDDP) and studied its second-order nonlinear optical (NLO) properties.[11] It was found, using 1064 nm nanosecond laser pulses, that the crystalline powder of DDDDP displays a very high second harmonic generation (SHG) efficiency.[11] This was the first SHG study for a

[a] *Department of Theoretical Physics, Faculty of Fundamental Problems of Technology, Wrocław University of Science and Technology, Wyb. Wyspiańskiego 27, PL-50370, Wrocław, Poland*
[b] *Department of Chemistry, Indian Institute of Technology Bhilai, Sejbahar, Raipur, Chhattisgarh, 492015, India. E-mail: mehboob@iitbhilai.ac.in*
[c] *Faculty of Chemistry, Wrocław University of Science and Technology, Wyb. Wyspiańskiego 27, PL-50370, Wrocław, Poland. E-mail: robert.zalesny@pwr.edu.pl*

† Electronic supplementary information (ESI) available. See DOI: https://doi.org/10.1039/d2cp00381c

propellane-based system. These promising experimental results for a single propellane and the on-going quest for second-order NLO materials[20] motivated the present theoretical work, in which we wish to study the molecular first hyperpolarizability for larger sets of propellane derivatives. In particular, we aim to establish ''structure–property'' relationships using a palette of substituents at different positions. To that end, we employed several state-of-the-art theoretical approaches combined with electronic- and vibrational-structure calculations. In fact, computer simulations provide an invaluable tool in the analysis of second-order nonlinear optical properties of molecules and their assemblies.[21–29]

2 Theory and computational methods

In the presence of an electric field (F), the Cartesian component of the total dipole moment μ_i may be expressed as a Taylor series:[30]

$$\begin{aligned}\mu_a(\omega_\sigma) &= \mu_a^0 + \sum_b \alpha_{ab}(-\omega_\sigma;\omega_1)F_b(\omega_1) + \\ &\frac{1}{2!}K^{(2)}\sum_{bc}\beta_{abc}(-\omega_\sigma;\omega_1,\omega_2)F_b(\omega_1)F_c(\omega_2) + \\ &\frac{1}{3!}K^{(3)}\sum_{bcd}\gamma_{abcd}(-\omega_\sigma;\omega_1,\omega_2,\omega_3)F_b(\omega_1)F_c(\omega_2)F_d(\omega_3) + \ldots\end{aligned} \quad (1)$$

where μ_a^0 is the a-th component of the permanent dipole moment; α_{ab}, β_{abc} and γ_{abcd} are the components of the molecular polarizability, and first and second hyperpolarizability tensors, respectively. ω_σ is the sum of the interacting fields with frequencies ω_i; and $K^{(2)}$ and $K^{(3)}$ are factors ensuring that all hyperpolarizabilities of the same order have the same static limit. Using perturbation theory, the (hyper)polarizabilities can be expressed as a sum-over all the states of the system (in general rovibronic). In this work, we are interested in the first hyperpolarizability, whose general sum-over-states expression is given as[31]

$$\beta_{abc}(-\omega_\sigma;\omega_1,\omega_2) = \sum \mathscr{P}_{-\omega_\sigma,\omega_1,\omega_2}\sum_{m,n}{}'\frac{\mu_a^{0m}\bar{\mu}_b^{mn}\mu_c^{n0}}{(E_{0m}-E_\sigma)(E_{0n}-E_2)} \quad (2)$$

where $\mathscr{P}_{-\omega_\sigma,\omega_1,\omega_2}$ represents the summation over all the permutations of the pairs $(a,-\omega_\sigma)$, (b,ω_1), and (c,ω_2) and $E_i = \hbar\omega_i$ $(i = 1, 2, \sigma)$. The prime over the double summation in eqn (2) represents a restricted summation where none of the indices could label the ground state. E_{mn} and μ_a^{mn} stand for the excitation energy and ath component of the transition dipole moment for $m \rightarrow n$ transition, respectively. Note that $\bar{\mu}^{mn} = \bar{\mu}^{mn} - \mu^{00}$. The static limit of the tensor components can be obtained by setting all three angular frequencies to zero. The commonly used first hyperpolarizability, $\beta_\parallel$, can be calculated from the β_{abc} components using the following relation:[32]

$$\beta_\parallel = \frac{1}{5}\sum_{a,b}(\beta_{abb}+\beta_{bab}+\beta_{bba})\bar{\mu}_a^{00} \quad (3)$$

In the above equations $\bar{\mu}_a^{00}$ stands for the ground-state dipole unit in the direction of the ground-state dipole moment ($\mu_a^{00}/|\mu^{00}|$).

Within the Born–Oppenheimer (BO) approximation, the molecular (hyper)polarizabilities defined by eqn (1) may be separated into pure electronic (P^e) and pure vibrational (P^v) contributions, as well as the zero-point vibrational averaging (ZPVA) correction:[32]

$$P = P^e + P^v + P^{\mathrm{ZPVA}} \quad (4)$$

where $P = \alpha, \beta, \gamma$. Alternatively, one can divide the property P into electronic, nuclear relaxation (P^{nr}) and curvature (P^{curv}) contributions:[32]

$$P = P^{\mathrm{curv}} + P^{\mathrm{nr}} + P^{\mathrm{curv}} \quad (5)$$

The latter separation is employed in this study and we only focus on the nuclear relaxation contribution to first hyperpolarizability. The P^{nr} terms are usually larger than P^{curv} terms. In order to treat the effect of molecular vibrations on electric properties, Bishop and Kirtman proposed a double (electrical and mechanical) perturbation theory (BKPT) treatment.[33] The P^{nr} contributions are given by the leading terms of each type of ''square bracket'' term of BKPT pure vibrational contributions. Within this approach, the nuclear relaxation first and second hyperpolarizability may be expressed in the ''square bracket'' notation as:

$$\beta^{\mathrm{nr}} = [\mu\alpha]^{(0,0)} + [\mu^3]^{(1,0)} + [\mu^3]^{(0,1)} \quad (6)$$

Each square bracket involves products of the normal coordinate derivatives of the electronic electrical properties indicated, as well as harmonic vibrational frequencies and anharmonic force constants. Each term is labeled by a pair of superscripts (p, q) denoting the order in electrical and mechanical anharmonicities, respectively. There is an efficient finite-field nuclear relaxation method (FF-NR)[34,35] for computing nuclear relaxation hyperpolarizabilities. However, in this study the field-induced coordinates (FICs) approach is used[36,37] to determine the anharmonicity contributions to nuclear relaxation first hyperpolarizability. FICs are linear combinations of field-free normal coordinates associated with the change in equilibrium geometry induced by a static electric field. The displacement of the i-th field-free normal coordinate at the field-relaxed geometry is given by:[36]

$$\begin{aligned}Q_i^F(F_x,F_y,F_z) = &-\sum_a^{x,y,z} q_1^{i,a}F_a - \sum_{a,b}^{x,y,z}\left[q_2^{i,ab} - \sum_{j=1}^{3N-6}\frac{a_{21}^{ij,a}}{a_{20}^{ii}}q_1^{i,b}\right. \\ &\left. + \sum_{j,k=1}^{3N-6}\frac{3a_{30}^{ijk}}{2a_{20}^{ii}}q_1^{j,a}q_1^{k,b}\right]F_aF_b + \ldots\end{aligned} \quad (7)$$

where,

$$a_{nm}^{ij\ldots ab\ldots} = \frac{1}{n!m!}\left(\frac{\partial^{(n+m)}V(Q_1,\ldots,Q_{3N-6},F_x,F_y,F_z)}{\partial Q_i\partial Q_j\cdots\partial F_a\partial F_b\cdots}\right)_{Q=0,\,F=0} \quad (8)$$

and

$$q_1^{i,a} = \frac{a_{11}^{i,a}}{2a_{20}^{ii}}, \quad q_2^{i,ab} = \frac{a_{12}^{i,ab}}{2a_{20}^{ii}} \tag{9}$$

The indices i,j and k stand for normal coordinates whereas a and b label the Cartesian directions. $a_{nm}^{ij\ldots ab\ldots}$ involves the n-th and m-th derivatives of the potential energy $V(Q,F)$ with respect to normal coordinates and field components, respectively. The first-order FICs:

$$\chi_1^a = -\sum_{i=1}^{3N-6} q_1^{i,a} Q_i \tag{10}$$

are sufficient to compute the static nuclear relaxation contribution to first hyperpolarizability:[36]

$$\beta_{abc}^{\mathrm{nr}}(0;0,0) = \sum_{i=1} P_{abc} a_{12}^{i,ab} q_1^{i,c} - \sum_{i,j=1} P_{abc} a_{21}^{ij,a} q_1^{i,b} q_1^{j,c} + \sum_{i,j,k=1} P_{abc} a_{30}^{ijk} q_1^{i,a} q_1^{j,b} q_1^{k,c} \tag{11}$$

$\sum P_{ab\ldots}$ indicates the sum over all permutations of the indices $a, b, \ldots$

Electronic and vibrational structure calculations, assuming C_2 symmetry point group for all compounds but one, were performed with the Gaussian suite of programmes.[38] To that end we used the range-separated CAM-B3LYP functional[39] and the aug-cc-pVDZ basis set.[40] The choice of this functional is dictated by its satisfactory performance in predicting electronic and vibrational contributions to the electric properties of various orders.[41–44] The results of these calculations were used for computing vibrational hyperpolarizabilities using custom computer routines. Additionally, the components of static electronic β and different transition dipole moments were calculated using the LSDALTON programme package using the CAM-B3LYP/6-31+G level of theory to study the convergence of β with the number of electronic states based on the generalized few-state model (GFSM).[45] The GFSM calculations were performed using in-house code.

3 Results and discussion

The structures of all the sixteen compounds studied in this work are given in Fig. 1. All these molecules are propellane derivatives with three wings: one consisting of unsubstituted cyclohexane, and the other two are identical benzo-oxazine moieties. The two benzo-oxazine wings are substituted with various groups such as $-NH_2$, $-CF_3$ (mono- and di-), $-SCH_3$, $-SO_2CH_3$, $-SCF_3$, $-OCF_3$, dioxolane, $-CH_2OCH_3$, and $-NO_2$ yielding a set composed of 16 compounds (Fig. 1). The methodology of preparation of this type of compound, based on the reaction of cyclic 1,2-diketones and *ortho*-aminophenols has

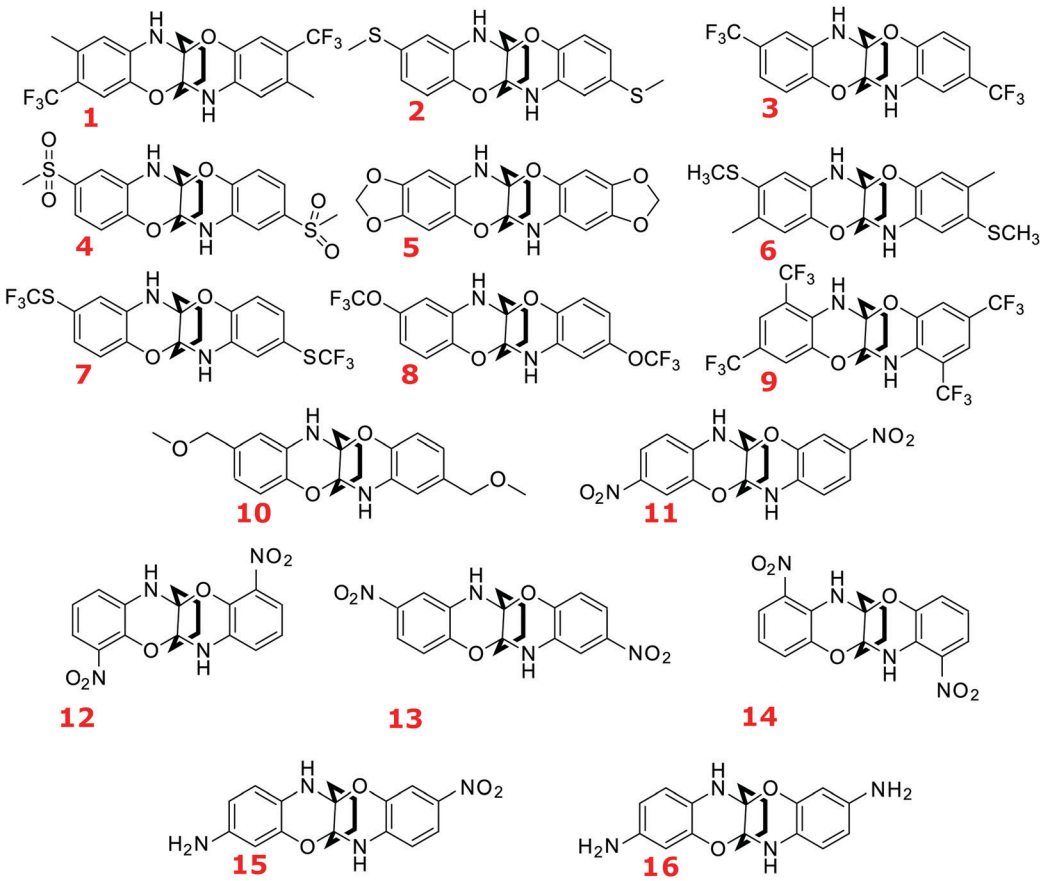

Fig. 1 Compounds studied in this work and their labelling.

been already developed and it can be adapted for the synthesis of most promising derivatives. The whole series of compounds, except **5**, can be divided into three major categories covering a wide range of Hammett substituent constants:[46] (a) Singly-substituted compounds (at each wing) in the *para* position in relation to the ether oxygen; their order in the series can be established according to the electron-accepting capabilities of the substituent: **13** (–NO_2, substituent constant is 0.78) **4** (–SO_2CH_3, 0.72), **3** (–CF_3, 0.54), **7** (–SCF_3, 0.50), **8** (–OCF_3, 0.35), **10** (–CH_2OCH_3, 0.01), **2** (–SCH_3, 0.00). (b) Singly-substituted compounds (at each wing) in positions other than *para*: **11** (*m*-NO_2, 0.71), **12**, and **14**; **15** (*m*-NH_2, −0.16 and *m*-NO_2, 0.71) and **16** (*m*-NH_2, −0.16). (c) Doubly-substituted compounds (on each wing): **1** (*p*-CH_3, −0.17 and *m*-CF_3, 0.43), **6** (*p*-SCH_3, 0.00 and *m*-CH_3, −0.07), **9** (two *m*-CF_3 groups, 0.43). It is worth pointing out that the oxygen atom was chosen as a "standard" because its electronegativity is higher than that of nitrogen (NH group). Note that the experimentally studied DDDDP molecule[11] is also included in the set shown in Fig. 1 (as compound **11**).

The values of electronic first hyperpolarizability ($\beta_\parallel^{e}$) for all the compounds calculated using the aug-cc-pVDZ basis set and CAM-B3LYP functional are presented in Table 1. We will start the discussion with the purely electronic counterpart as it contributes significantly to second-order processes involving both static and dynamic fields. Compound **11** has the maximum value for $\beta_\parallel^{e}$ and compound **16** has the least value (in magnitude). The ratio between the maximum and minimum values of $\beta_\parallel^{e}$ is 54 : 1. The compound with the second largest $\beta_\parallel^{e}$ is **15**, which is the only compound asymmetrically substituted (–NO_2 and –NH_2) at *para* positions. We note that the replacement of one electron-accepting group with an electron-donating one, while preserving the positions of the substituents, does not lead to deterioration of the electronic first hyperpolarizability. It is interesting to note that compounds **1**, **3** and **9** have almost the same values for $\beta_\parallel^{e}$ indicating that there is almost no effect of adding an extra –CF_3 group or changing the position of the –CF_3 group in the benzo-oxazine wings. Similarly, compounds **2** and **6** have similar values for $\beta_\parallel^{e}$ indicating that there is no effect of adding an extra methyl group in the benzo-oxazine ring. On replacing –SCH_3 by –CF_3, *i.e.*, on moving from compound **2** to **3**, there is an increase in $\beta_\parallel^{e}$ value. Replacing –CF_3 by –OCF_3 (compound **3** to compound **8**) leaves the $\beta_\parallel^{e}$ values practically unchanged and replacing –CF_3 by –SCF_3, *i.e.*, on moving from compound **3** to **7**, the $\beta_\parallel^{e}$ values are almost doubled. This is probably because of the available vacant d-orbital on the S-atom. On replacing –SCH_3 (compound **2**) by –SO_2CH_3 (compound **4**) there is about a three-fold increase in the $\beta_\parallel^{e}$ values and replacing –SCH_3 (compound **2**) by –SCF_3 (compound **7**) there is a corresponding 2.5-fold increase. Compounds **12** and **14** show a variation in $\beta_\parallel^{e}$ which emphasizes the importance of substituent placement. Finally, let us recall that compound **16** has two electron-donating substituents at the *meta* position and exhibits the smallest $\beta_\parallel^{e}$ value. Such substituent placement maximizes $\beta_\parallel^{e}$ but only for strong electron-donating groups.

In order to shed light on large values of $\beta_\parallel^{e}$ found for **11**, we employed the corresponding generalized few-state model (GFSM) developed by some of the current authors.[45] Within GFSM, the expression for $\beta_\parallel^{e}$ is given as[45]

$$\beta_\parallel^{\mathrm{GFSM}} = \frac{1}{5}\sum_{m,n}{}' \beta_{mn} = \frac{1}{5}\sum_{m,n}{}' \frac{D_{mn}}{E_{mn}} \times A_{mn} \tag{12}$$

where

$$\begin{aligned} D_{mn} &= \mu^{0m}\bar{\mu}^{mn}\mu^{n0} \\ A_{mn} &= \cos\theta_{0m}^{00}\cos\theta_{mn}^{0n} + \cos\theta_{0m}^{mn}\cos\theta_{0n}^{00} + \cos\theta_{0m}^{0n}\cos\theta_{mn}^{00} \end{aligned} \tag{13}$$

and for the static case,

$$E_{mn} = \frac{E_{0m}E_{0n}}{6} \tag{14}$$

and θ_{ab}^{cd} is the angle between transition dipole moments μ^{ab} and μ^{cd}. The prime in eqn (12) indicates a restricted summation, where the ground state is not included. Other terms have their usual meanings. Each $\beta_{mn}^{\mathrm{GFSM}}$ can either be positive or negative depending on the values of A_{mn}, *i.e.*, the relative orientation of the involved transition dipole moment vectors. We have included up to 50 excited states in GFSM calculations. The convergence of $\beta_\parallel^{e}$ with the number of states involved in GFSM for **11** is shown in Fig. 2. The corresponding data for some other studied propellanes are presented in Fig. S1 in the ESI† file and allow for drawing a conclusion that $\beta_\parallel^{e}$ is slowly convergent with respect to the number of electronic excited states, thus indicating that there are no key electronic states determining the first hyperpolarizability. In contrast, the results shown in Fig. 2 for **11** indicate that GFSM is quite successful in the quantitative prediction of $\beta_\parallel^{e}$ values, including its sign.

We have noticed that involving all the 50 excited states gives $\beta_\parallel^{\mathrm{GFSM}}$ = 1642 au, 75% of which is contributed by the top five positive and the top five negative terms. β_{mn} as well as the

Table 1 Vectorial electronic and harmonic vibrational contributions to the first hyperpolarizability (in au) computed at the CAM-B3LYP/aug-cc-pVDZ level

Compound	$\beta_\parallel^{e}$	$[\mu\alpha]_\parallel^{(0,0)}$	Sum
1	196	3053	3249
2	218	1814	2032
3	246	3291	3537
4	−521	−5997	−6518
5	112	538	650
6	247	1442	1689
7	534	3307	3841
8	212	2839	3051
9	251	3358	3609
10	449	−1481	−1032
11	1198	7330	8528
12	368	3060	3428
13	710	5862	6572
14	214	−226	−12
15	1087	6896	7983
16	22	−2117	−2095

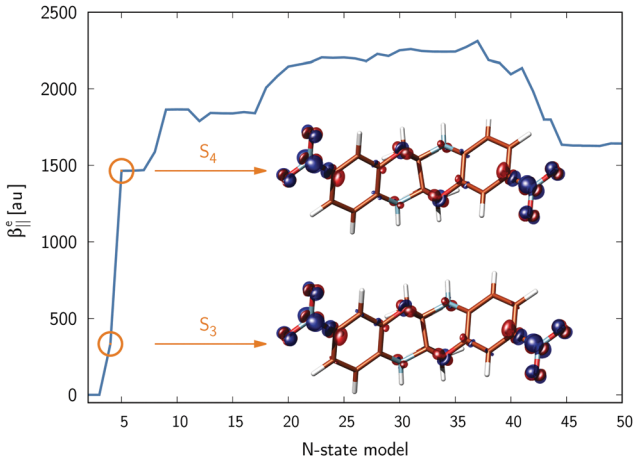

Fig. 2 Convergence of the electronic first hyperpolarizability for **11** with the number of electronic states (*N*-state model accounts also for electronic ground state). The inset shows the electronic density difference ($\Delta\rho$ (r)) between electronic singlet state ρ (r, S_i) and the ground electronic state ρ (r, S_0). The contour value of density was set at 0.005 au and positive (negative) values of $\Delta\rho$ (r) are represented by blue (red) color. Calculations were performed at the CAM-B3LYP/6-31+G level.

corresponding dipole (D_{mn}), angle (A_{mn}), and energy (E_{mn}) terms are given in Table 2.

It is interesting to note that the large positive terms, *i.e.*, β_{33}, β_{34}, and β_{44} have the largest dipole contributions. The first two have an angle term $\sim$1, whereas the last one has an angle term equal to 3 (which is maximum). The dipole contribution in β_{44} is less than half of those in either β_{33} or β_{34}, but the corresponding maximum angle contribution makes it the largest contributing β_{mn}. The character of two key electronic states (S_3 and S_4) is shown in the inset in Fig. 2 – there is a symmetric density shift from 1,4-oxazine moieties towards nitro groups. The angles between each pair of contributing transition dipole moments are presented in Table 3, which clearly indicates that in β_{44} and β_{88} all the transition dipole moments are aligned parallel to each other making the angular contribution the maximum. In the group of negative β_{mn} contributors, one of the pairs of transition dipole moments makes an angle larger than 90 leading to an overall negative term. Among all the major negative contributors, the dipole contributions are very small and the corresponding energy contributions are slightly higher than the positive β_{mn} and hence for compound **11** $\beta_{\|}^{e}$ is the largest. Let us close this section highlighting that although the GFSM analysis was performed using 6-31+G basis, the data in Table S1 in the ESI† file indicate that there is a satisfactory agreement with property values obtained with the larger aug-cc-pVDZ basis set.

Table 2 Largest β_{mn}^{GFSM} terms for compound **11** computed at the CAM-B3LYP/6-31 + G level

m, n	$\beta_{mn} = \beta_{nm}$	D_{mn}	A_{mn}	$5.0 \times E_{mn}$
3, 3	333	6.3544	1.0	0.0191
3, 4	327	6.4129	0.98	0.0192
4, 4	477	3.0659	3.0	0.0193
3, 11	−40	1.4270	−0.7	0.0251
4, 11	−70	1.8760	−0.94	0.0252
4, 12	−51	0.4353	−3.0	0.0255
8, 8	81	0.6591	3.0	0.0245

Table 3 Angle between transition dipole moments involved in major β_{mn} terms

β_{mn}	a	b	c	d	θ_{ab}^{cd}	β_{mn}	a	b	c	d	θ_{ab}^{cd}
β_{33}	0	0	0	3	90	β_{311}	0	11	3	11	90
	0	0	3	3	0		0	3	3	11	90
	0	3	3	3	90		0	11	0	0	90
β_{34}	0	4	3	4	90		0	3	0	11	45
	0	3	3	4	12		0	0	3	11	180
	0	0	0	4	0	β_{411}	0	11	4	11	160
	0	3	0	4	90		0	4	4	11	90
	0	0	3	4	90		0	4	0	11	90
β_{44}	0	0	4	4	0		0	0	4	11	90
	0	4	4	4	0	β_{412}	0	12	4	12	180
β_{88}	0	0	0	8	0		0	4	4	12	180
	0	0	8	8	0		0	12	0	0	0
	0	8	8	8	0		0	4	0	12	0
							0	0	4	12	180

We will now turn to the analysis of vibrational contributions to the first hyperpolarizability. In order to gain an insight into their importance to the static property, we have computed the purely harmonic term, as defined by eqn (6), for **1–16**. The results are assembled in Table 1 and demonstrate that the $[\mu\alpha]_{\|}^{(0,0)}$ term prevails over the electronic counterpart and in many cases the ratio reaches up to the factor of 10. Similarly to what has been demonstrated for the purely electronic $\beta_{\|}^{e}$ term, the largest harmonic vibrational counterpart is found for **11**. On passing from electronic contributions to the sum of electronic and vibrational terms, the property-based ordering of compounds changes, albeit the largest value is found in both cases for **11**. It should be highlighted that we consider here frequency-independent first hyperpolarizability and the vibrational contributions become less significant for dynamic fields. However, if at least one static field is involved, they might add a substantial contribution to the overall second-order nonlinear optical response.[47] In what follows we will analyze in more detail compounds **11** as well **12–14** with the NO_2 group placed at various positions. Table 4 and Fig. 3 show lowest-order anharmonic terms contributing to $\beta_{\|}$. Three major conclusions can be drawn from these data, namely: (i) both electrical and mechanical anharmonicities make a substantial contribution to the vibrational counterpart (*e.g.*, for compound **11** the absolute value of the (1,0) term is 40% of (0,0)), (ii) anharmonic corrections may significantly reduce the purely harmonic term, as they are of opposite signs (see *e.g.* **11**), and (iii) there is no clear pattern of the electrical and mechanical anharmonicities

Table 4 Breakdown of vibrational first hyperpolarizability (in au) into anharmonic terms

Compound	$[\mu^3]_{\|}^{(1,0)}$	$[\mu^3]_{\|}^{(0,1)}$	$[\mu^3]_{\|}^{(1,0)} + [\mu^3]_{\|}^{(0,1)}$
11	−2959	−1258	−4217
12	−655	1148	493
13	808	−2078	−1270
14	1052	−622	430

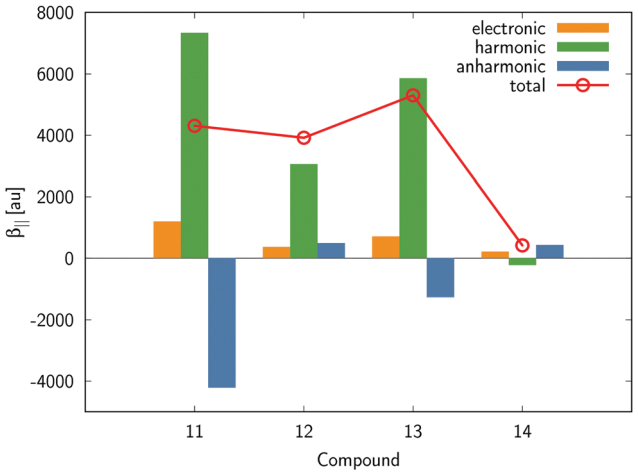

Fig. 3 Breakdown of $\beta_{\|}$ for **11–14** into electronic and vibrational contributions.

for compounds **11–14**. It should be thus concluded that for static hyperpolarizability these terms should be evaluated explicitly as they might have a significant effect on overall trends in $\beta_{\|}$.

In what follows we will analyze in more detail the origins of large harmonic vibrational hyperpolarizability for compound **11**. Fig. 4 shows the orientation of compound **11** in the cartesian coordinate system (note that the two-fold symmetry axis is parallel to the cartesian z direction). The breakdown of $[\mu\alpha]_{\|}^{(0,0)}$ into symmetry-unique non-vanishing cartesian components is presented in Fig. 5. As seen, the cartesian zzz component parallel to the symmetry axis is by far the largest. In order to link this component with the vibrational structure of **11** we performed the sum-over-normal modes calculations and the results are shown in Fig. 6. It is clear that the first normal mode with wavenumber 17 cm^{-1} makes the dominant contribution (91% of $[\mu\alpha]_{zzz}^{(0,0)}$). Atomic displacements for the normal mode in question show the symmetric vibrations of the propellane wings (see Fig. 4). For propellane molecule **11**, in a noncentrosymmetric crystal structure with the z-axis parallel to the

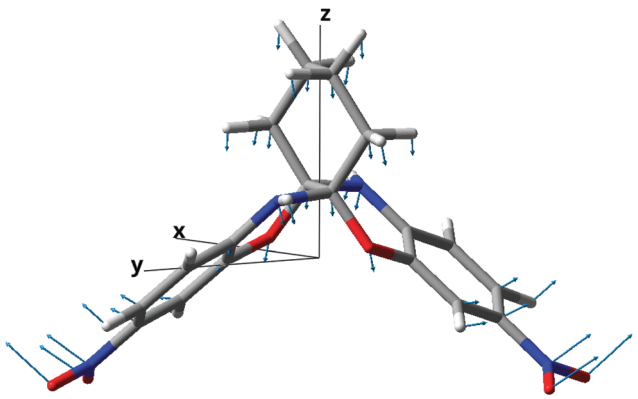

Fig. 4 The orientation of compound **11** in the cartesian coordinate system. Atomic displacements corresponding to the lowest-frequency normal mode are indicated by arrows.

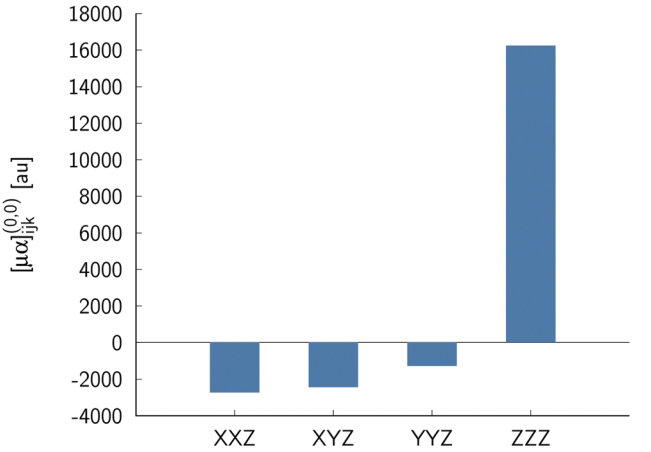

Fig. 5 Cartesian components of harmonic vibrational hyperpolarizability (in au) for compound **11**.

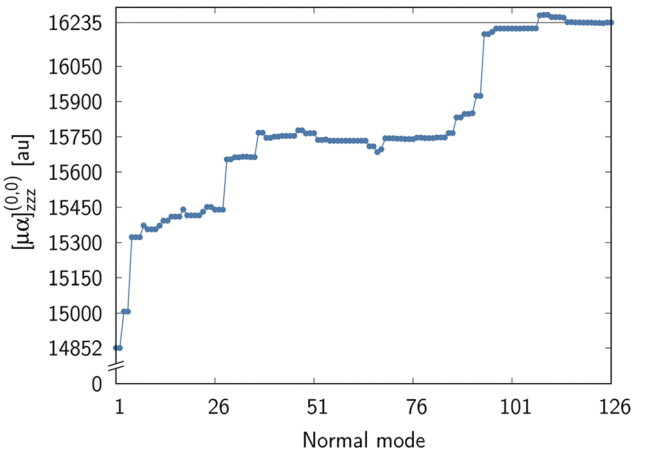

Fig. 6 Convergence of the zzz component of harmonic vibrational hyperpolarizability (in au) for compound **11**.

crystal polar axis,[11] the existence of such "butterfly motion" polar mode could be beneficial for the crystal electrooptic properties, especially in the THz frequency range.[48] Strong second-order nonlinear optical properties of organic crystals, *e.g.*, such as found for DAST crystals,[49,50] can be exploited for both generation and detection of THz radiation. Organic crystals possessing high THz-generation efficiencies are highly desired for THz spectroscopy, imaging and analysis due to unique penetration properties of THz radiation.[51,52]

4 Conclusions

Aiming to establish "structure–property" relations, in this work we have employed computational quantum chemistry methods to study first order hyperpolarizabilities of 16 propellanes. In particular, we considered a wide palette of symmetrically-placed substituents (–CF_3, –SCH_3, –SO_2CH_3, –SCF_3, –OCF_3, –CH_2OCH_3, dioxolane and –NO_2) which cover a wide range of values of Hammett substituent constants. It has been

demonstrated that the maximum values of frequency-independent first hyperpolarizability can be obtained for strong electron-accepting NO_2 substituents but only at the preferred positions with respect to the electronegative oxygen atom in the 1,4-oxazine moiety. This holds for electronic as well as vibrational counterparts. However, asymmetric substitution with NO_2 and NH_2 groups at these preferred positions (compound **15**) leads to equally high electronic and vibrational hyperpolarizability values. The variations in computed properties are large among the studied set of substituents and can reach an order of magnitude. In order to shed light on these findings, we employed a generalized few state model to study the electronic counterpart. It turned out that the overall convergence of the first hyperpolarizability with respect to the number of electronic states is slow, indicating a complicated origin of this property. Some of the studied herein propellanes (**7**, **10**, **13**), due to similar molecular structure with compound **11** and large values of their first hyperpolarizabilities can be considered as promising candidates for synthesis, crystal growth and the evaluation of their second order NLO properties, providing that they will crystallize in noncentrosymmetric point groups.

Conflicts of interest

There are no conflicts to declare.

Acknowledgements

The authors cordially thank Miss Elizaveta F. Petrusevich for the preparation of the graphical abstract. The authors acknowledge the Wroclaw Center for Networking and Supercomputing for granting computational resources. MMA acknowledges the research initiation grant from IIT Bhilai.

References

1 G. Snatzke and G. Zanati, *Justus Liebigs Ann. Chem.*, 1965, **684**, 62–78.
2 O. Diels and W. Friedrichsen, *Justus Liebigs Ann. Chem.*, 1934, **513**, 145–155.
3 G. Wittig and U. Mayer, *Chem. Ber.*, 1963, **96**, 342–348.
4 J. Altman, E. Babad, J. Itzchaki and D. Ginsburg, *Tetrahedron*, 1966, **22**, 279–304.
5 A. M. Dilmaç, E. Spuling, A. de Meijere and S. Bräse, *Angew. Chem., Int. Ed.*, 2017, **56**, 5684–5718.
6 A. M. Dilmaç, T. Wezeman, R. M. Bär and S. Bräse, *Nat. Prod. Rep.*, 2020, **37**, 224–245.
7 J. Kanazawa and M. Uchiyama, *Synlett*, 2019, 1–11.
8 F. Reuß and P. Heretsch, *Angew. Chem., Int. Ed.*, 2020, **59**, 10232–10234.
9 F.-S. He, S. Xie, Y. Yao and J. Wu, *Chin. Chem. Lett.*, 2020, **31**, 3065–3072.
10 M. M.-D. Pramanik, H. Qian, W.-J. Xiao and J.-R. Chen, *Org. Chem. Front.*, 2020, **7**, 2531–2537.
11 A. Miniewicz, S. Bartkiewicz, E. Wojaczyńska, T. Galica, R. Zaleśny and R. Jakubas, *J. Mater. Chem. C*, 2019, **7**, 1255–1262.
12 X.-Y. Liu, X. Tang, Y. Zhao, D. Zhao, J. Fan and L.-S. Liao, *ACS Appl. Mater. Interfaces*, 2018, **10**, 1925–1932.
13 K. B. Wiberg and S. T. Waddell, *J. Am. Chem. Soc.*, 1990, **112**, 2194–2216.
14 K. C. Nicolaou, J. Yin, D. Mandal, R. D. Erande, P. Klahn, M. Jin, M. Aujay, J. Sandoval, J. Gavrilyuk and D. Vourloumis, *J. Am. Chem. Soc.*, 2016, **138**, 1698–1708.
15 J. Kaleta, Z. Janoušek, M. Nečas and C. Mazal, *Organometallics*, 2015, **34**, 967–972.
16 P. R. Khoury, J. D. Goddard and W. Tam, *Tetrahedron*, 2004, **60**, 8103–8112.
17 K. Jug and A. Poredda, *J. Am. Chem. Soc.*, 1991, **113**, 761–764.
18 D. Nied, W. Klopper and F. Breher, *Angew. Chem., Int. Ed.*, 2009, **48**, 1411–1416.
19 F. Zerbetto, *Chem. Phys. Lett.*, 1995, **241**, 445–449.
20 F. Castet, V. Rodriguez, J.-L. Pozzo, L. Ducasse, A. Plaquet and B. Champagne, *Acc. Chem. Res.*, 2013, **46**, 2656–2665.
21 C. Bouquiaux, C. Tonnelé, F. Castet and B. Champagne, *J. Phys. Chem. B*, 2020, **124**, 2101–2109.
22 J. Seibert, B. Champagne, S. Grimme and M. de Wergifosse, *J. Phys. Chem. B*, 2020, **124**, 2568–2578.
23 C. Bouquiaux, F. Castet and B. Champagne, *J. Phys. Chem. B*, 2021, **125**, 10195–10212.
24 J. Quertinmont, L. Maschio, A. Datta and B. Champagne, *J. Phys. Chem. C*, 2020, **124**, 24451–24459.
25 E. Rtibi and B. Champagne, *Symmetry*, 2021, **13**, 1636.
26 K. Pielak, F. Bondu, L. Sanguinet, V. Rodriguez, F. Castet and B. Champagne, *Dyes Pigm.*, 2019, **160**, 641–646.
27 F. Castet, A. Gillet, F. Bureš, A. Plaquet, V. Rodriguez and B. Champagne, *Dyes Pigm.*, 2021, **184**, 108850.
28 T. N. Ramos, S. Canuto and B. Champagne, *J. Chem. Inf. Model.*, 2020, **60**, 4817–4826.
29 P. Beaujean, B. Champagne, S. Grimme and M. de Wergifosse, *J. Phys. Chem. Lett.*, 2021, **12**, 9684–9690.
30 D. P. Shelton and J. E. Rice, *Chem. Rev.*, 1994, **94**, 3–29.
31 B. J. Orr and J. F. Ward, *Mol. Phys.*, 1971, **20**, 513–526.
32 D. M. Bishop, *Adv. Chem. Phys.*, 1998, **104**, 1–40.
33 D. M. Bishop and B. Kirtman, *J. Chem. Phys.*, 1991, **95**, 2646.
34 D. M. Bishop, M. Hasan and B. Kirtman, *J. Chem. Phys.*, 1995, **103**, 4157–4159.
35 J. M. Luis, M. Duran, J. L. Andrés, B. Champagne and B. Kirtman, *J. Chem. Phys.*, 1999, **111**, 875–884.
36 J. M. Luis, M. Duran, B. Champagne and B. Kirtman, *J. Chem. Phys.*, 2000, **113**, 5203–5213.
37 J. M. Luis, M. Duran and B. Kirtman, *J. Chem. Phys.*, 2001, **115**, 4473–4483.
38 M. J. Frisch, G. W. Trucks, H. B. Schlegel, G. E. Scuseria, M. A. Robb, J. R. Cheeseman, G. Scalmani, V. Barone, B. Mennucci, G. A. Petersson, H. Nakatsuji, M. Caricato, X. Li, H. P. Hratchian, A. F. Izmaylov, J. Bloino, G. Zheng, J. L. Sonnenberg, M. Hada, M. Ehara, K. Toyota, R. Fukuda, J. Hasegawa, M. Ishida, T. Nakajima, Y. Honda, O. Kitao, H. Nakai, T. Vreven, J. A. Montgomery Jr., J. E. Peralta,

F. Ogliaro, M. Bearpark, J. J. Heyd, E. Brothers, K. N. Kudin, V. N. Staroverov, R. Kobayashi, J. Normand, K. Raghavachari, A. Rendell, J. C. Burant, S. S. Iyengar, J. Tomasi, M. Cossi, N. Rega, J. M. Millam, M. Klene, J. E. Knox, J. B. Cross, V. Bakken, C. Adamo, J. Jaramillo, R. Gomperts, R. E. Stratmann, O. Yazyev, A. J. Austin, R. Cammi, C. Pomelli, J. W. Ochterski, R. L. Martin, K. Morokuma, V. G. Zakrzewski, G. A. Voth, P. Salvador, J. J. Dannenberg, S. Dapprich, A. D. Daniels, O. Farkas, J. B. Foresman, J. V. Ortiz, J. Cioslowski and D. J. Fox, *Gaussian 09 Revision D.01*, Gaussian Inc.; Wallingford CT, 2009.

39 T. Yanai, D. P. Tew and N. C. Handy, *Chem. Phys. Lett.*, 2004, **393**, 51–57.

40 T. H. Dunning, *J. Chem. Phys.*, 1989, **90**, 1007–1023.

41 R. Zaleśny, I. W. Bulik, W. Bartkowiak, J. M. Luis, A. Avramopoulos, M. G. Papadopoulos and P. Krawczyk, *J. Chem. Phys.*, 2010, **133**, 244308.

42 I. W. Bulik, R. Zaleśny, W. Bartkowiak, J. M. Luis, B. Kirtman, G. E. Scuseria, A. Avramopoulos, H. Reis and M. G. Papadopoulos, *J. Comput. Chem.*, 2013, **34**, 1775–1784.

43 A. Baranowska-Łaczkowska, W. Bartkowiak, R. W. Góra, F. Pawłowski and R. Zaleśny, *J. Comput. Chem.*, 2013, **34**, 819–826.

44 R. Zaleśny, M. Medved', S. Sitkiewicz, E. Matito and J. M. Luis, *J. Chem. Theory Comput.*, 2019, **15**, 3570–3579.

45 M. M. Alam, M. T.-P. Beerepoot and K. Ruud, *J. Chem. Phys.*, 2020, **152**, 244106.

46 C. Hansch, A. Leo and R. W. Taft, *Chem. Rev.*, 1991, **91**, 165–195.

47 D. M. Bishop, B. Kirtman, H. A. Kurtz and J. E. Rice, *J. Chem. Phys.*, 1993, **98**, 8024–8030.

48 M. Jazbinsek, U. Puc, A. Abina and A. Zidansek, *Appl. Sci.*, 2019, **9**, 882.

49 C. Bosshard, R. Spreiter, L. Degiorgi and P. Günter, *Phys. Rev. B: Condens. Matter Mater. Phys.*, 2002, **66**, 205107.

50 Z. Yang, L. Mutter, M. Stillhart, B. Ruiz, S. Aravazhi, M. Jazbinsek, A. Schneider, V. Gramlich and P. Günter, *Adv. Funct. Mater.*, 2007, **17**, 2018–2023.

51 Q. Sun, Y. He, K. Liu, S. Fan, E. P.-J. Parrott and E. Pickwell-MacPherson, *Quant. Imaging Med. Surg.*, 2017, **7**, 345–355.

52 B. Graber, C. Kim and D. H. Wu, *Appl. Phys. Lett.*, 2017, **111**, 221107.